Acta Mech 206, 207–224 (2009)
DOI 10.1007/s00707-008-0088-5

Y. Z. Chen · Z. X. Wang · X. Y. Lin

A new kernel in BIE and the exterior boundary value problem in plane elasticity

Received: 8 February 2008 / Revised: 27 June 2008 / Published online: 9 October 2008

Abstract A new kernel with formulation of the relevant BIE (boundary integral equation) in plane elasticity is introduced. The new kernel is derived from a fundamental solution expressed in a pure deformable form. If the kernel is used, the regularity condition is satisfied for any loadings on the contour of the hole. The exterior boundary value problem is studied. The applied loadings on the contour in the exterior boundary value problem may not be in equilibrium. From the solutions of the exterior von Neumann problem and the exterior Dirichlet problem, numerical examinations and comparison based on the usage of the new kernel and the usual kernel are presented. It is proved that the usual kernel cannot be used for the case in which the loadings on the contour are not in equilibrium. A particular exterior Dirichlet problem for an infinite plate with an elliptic inclusion is considered. Resultant forces and moment are applied on the inclusion. In the problem, one must assume some additional translation and rotation for the inclusion that are determined by the applied loading condition.

1 Introduction

The boundary integral equation (BIE) was widely used in elasticity, and the fundamental for BIE could be found in [1–3]. Heritage and early history of the boundary element method were summarized more recently [4].

Some problems in the BIE may not be studied throughout. One problem in this field is the degenerate scale problem [5–9]. In the degenerate scale problem, an improper solution to the Dirichet problem of BIE exists if the used size is near the critical value. In this paper, the used size for the studied configuration is sufficiently large. Therefore, the degenerate scale problem does not appear in the present study.

It is known that behavior for the solutions of the interior boundary value problem and the exterior boundary value problem in plane elasticity is quite different. For example, the applied loading on the contour must be in equilibrium in the interior problem. However, the applied loading on the contour may not be in equilibrium in the exterior problem.

Second, after using the Somigliana identity in the interior problem, the integration path (or boundary) in BIE is the outer boundary in the case of simply connected region. However, in the exterior boundary value problem, the integration paths (or boundaries) must be two boundaries. Among them, one is defined on the notch configuration and another is defined on a sufficiently large circle. The integral defined on the large circle is actually a mutual work difference integral (MWDI) [10]. The mentioned MWDIs on the large circle, $D^{*1}_{i(\mathrm{CR})}(\xi)$ and $D^{*2}_{i(\mathrm{CR})}(\xi)$, will be cited in Eqs. (20) and (25) below. If the mentioned MWDI $D^{*1}_{i(\mathrm{CR})}(\xi)$ or $D^{*2}_{i(\mathrm{CR})}(\xi)$ vanishes, the BIE can be further reduced to a simpler form. Otherwise, the BIE cannot

Y. Z. Chen (✉) · Z. X. Wang · X. Y. Lin
Division of Engineering Mechanics, Jiangsu University,
212013 Zhenjiang, Jiangsu, People's Republic of China
E-mail: chens@ujs.edu.cn
Tel.: +086-511-88780780
Fax: +086-522-88791739

be reduced further. The vanishing of the MWDI $D^{*1}_{i(\mathrm{CR})}(\xi)$ or $D^{*2}_{i(\mathrm{CR})}(\xi)$ is called the regularity condition in the literature [3]. The property of the mentioned MWDI, $D^{*1}_{i(\mathrm{CR})}(\xi)$ or $D^{*2}_{i(\mathrm{CR})}(\xi)$, mainly depends on the adopted form of the fundamental stress field and the property of the physical stress field.

This paper proposes a new kernel in BIE of plane elasticity. The exterior boundary value problem is studied. The new kernel is derived from a fundamental solution expressed in a pure deformable form. Theoretical analysis is carried out for the usage of the suggested new kernel and the usual kernel. It is proved that the regularity condition is satisfied for any loading condition on the contour if the suggested new kernel is used.

From the solutions of the exterior Neumann problem and exterior Dirichlet problem, numerical examinations and comparison based on the usage of the new kernel and the usual kernel are presented. Numerical examination proves that the new kernel can be used for the case in which the loadings on the contour are not in equilibrium. In addition, it proves that the usual kernel cannot be used for the case in which the loadings on the contour are not in equilibrium.

A particular exterior Dirichlet problem for an infinite plate with an elliptic inclusion is studied. Resultant forces and moment are applied on the inclusion. In the problem, one must assume some additional translation and rotation for the inclusion that are determined by the applied loading condition.

2 Different types of kernel from the fundamental solution with their BIE for the exterior problem

It is known that the BIE in plane elasticity is formulated on the fundamental solution with concentrated forces applied on a point in an infinite plane. Clearly, the relevant solutions for displacements from the fundamental solution can be different by a constant. If one chooses the displacements in pure deformable form, a new kernel $U^{*1}_{ij}(\xi, x)$ in the BIE is obtainable. The introduced kernel $U^{*1}_{ij}(\xi, x)$ (see Eq. (20) below) and relevant BIE are studied in detail. In addition, the usual kernel $U^{2}(\xi, x)$ (see Eq. (25) below) and relevant BIE are also studied.

2.1 Preliminary knowledge for the mutual work difference integral on a large circle

The preliminary knowledge for the MWDI on a large circle is important in the formulation of the BIE in the exterior boundary value problem [10,11]. This knowledge has a close relation with an integration term in the BIE.

The following analysis depends on the complex variable function method in plane elasticity [12]. In this method, the stresses $(\sigma_x, \sigma_y, \sigma_{xy})$, the resultant forces (X, Y) and the displacements (u, v) are expressed in terms of two complex potentials $\phi(z)$ and $\psi(z)$such that

$$\begin{aligned} \sigma_x + \sigma_y &= 4\mathrm{Re}\phi'(z), \\ \sigma_y - \sigma_x + 2\mathrm{i}\sigma_{xy} &= 2[\bar{z}\phi''(z) + \psi'(z)], \qquad (1) \\ f = -Y + \mathrm{i}X &= \phi(z) + z\overline{\phi'(z)} + \overline{\psi(z)}, \qquad (2) \\ 2G(u + \mathrm{i}v) &= \kappa\phi(z) - z\overline{\phi'(z)} - \overline{\psi(z)}, \qquad (3) \end{aligned}$$

where $z = x + \mathrm{i}y$ denotes a complex variable, G is the shear modulus of elasticity, $\kappa = (3 - \nu)/(1 + \nu)$ is for the plane stress problems, $\kappa = 3 - 4\nu$ is for the plane strain problems and ν is the Poisson's ratio. In the present study, the plane strain condition is assumed thoroughly. In the following, we occasionally rewrite the displacements u, v as u_1, u_2, σ_x, σ_y, σ_{xy} as σ_{11}, σ_{22}, σ_{12}, and x, y as x_1, x_2, respectively.

An important problem in plane elasticity is to evaluate an MWDI,which is a subtraction of two integrals from two stress fields [10,11].

In the case of remote tractions being zero, a physical stress field with the name of α-field is introduced, which is defined by two complex potentials [12]

$$\phi_{(\alpha)}(z) = A_2 \ln z + a_0 + \sum_{k=1}^{\infty} \frac{a_k}{z^k}, \quad \psi_{(\alpha)}(z) = B_2 \ln z + b_0 + \sum_{k=1}^{\infty} \frac{b_k}{z^k}, \qquad (4)$$

where

$$B_2 = -\kappa \bar{A}_2, \quad A_2 = -\frac{P_x + \mathrm{i}P_y}{2\pi(\kappa + 1)} \qquad (5)$$

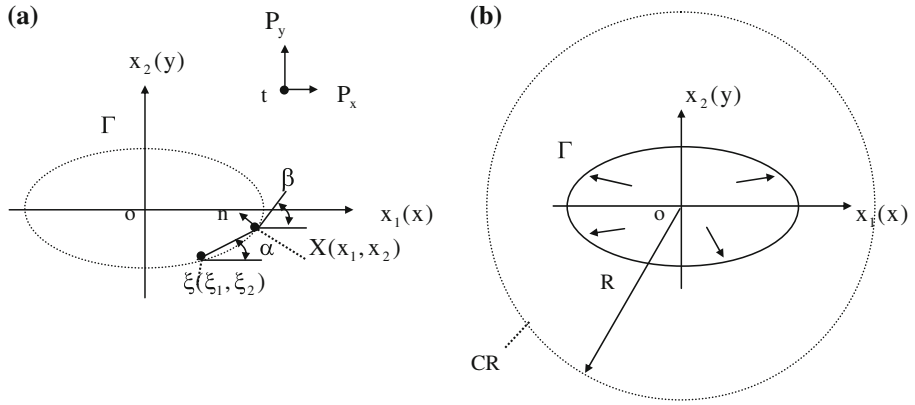

Fig. 1 **a** A concentrated force applied at the point $z = t$, or the loading condition for the α-field. **b** Some loadings having resultant forces applied on the elliptic contour, or the loading condition for the β-field

and $P_x + \mathrm{i}P_y$ denotes the resultant force applied in the finite portion of infinite plate. For some particular situation mentioned below, the α-field has been written in the impure deformable form. This can be seen from the fact that two pairs of complex potentials, the pair $\phi(z) = a_0$, $\psi(z) = 0$, and the pair $\phi(z) = 0$, $\psi(z) = b_0$, are involved in Eq. (4).

Secondly, another physical stress field with the name of β-field is introduced, which is defined by

$$\phi_{(\beta)}(z) = E_2 \ln z + \sum_{k=1}^{\infty} \frac{e_k}{z^k}, \quad \psi_{(\beta)}(z) = F_2 \ln z + \sum_{k=1}^{\infty} \frac{f_k}{z^k} \quad (\text{with } F_2 = -\kappa \bar{E}_2). \tag{6}$$

Note that the β-field represents the physical field in the following analysis, and it now has been expressed in the pure deformable form, or no constant terms are involved in $\phi_{(\beta)}(z)$ and $\psi_{(\beta)}(z)$. Alternatively speaking, each pair in Eq. (6) (for example, $\phi_{(\beta)}(z) = E_2 \ln z$, $\psi_{(\beta)}(z) = 0$) represents nonvanishing displacements and stresses anywhere.

After some manipulation, the following result for a path-independent integral was obtained [10]:

$$D_{(\mathrm{CR})} = \oint_{(\mathrm{CR})} \left(u_{i(\alpha)} \sigma_{ij(\beta)} - u_{i(\beta)} \sigma_{ij(\alpha)} \right) n_j \mathrm{d}s = -\frac{\pi(\kappa + 1)}{G} \mathrm{Re}[a_0 F_2 + b_0 E_2], \tag{7}$$

where CR is a sufficient large circle. It is valuable to describe the physical meaning of Eq. (7). In fact, the right hand term of Eq. (7) represents a contribution to the MWDI from the terms a_0, b_0 (representing the rigid translation in the α-field) and the terms F_2, E_2 (representing the resultant forces in the β-field). From Eq. (7), we see that, in the case of $F_2 \neq 0$, $E_2 \neq 0$, $a_0 = 0$, $b_0 = 0$ is a necessary condition for the condition $D_{(\mathrm{CR})} = 0$ to be satisfied.

The formulation of BIE in plane elasticity is introduced below. If the concentrated forces (P_x, P_y) is applied at the point $z = t$ (Fig. 1a) , the relevant complex potentials are defined by [12]

$$\phi_{(\alpha)}(z) = F \ln(z - t), \quad \psi_{(\alpha)}(z) = -\kappa \bar{F} \ln (z - t) - \frac{F\bar{t}}{z - t}, \tag{8}$$

where

$$F = -\frac{P_x + \mathrm{i}P_y}{2\pi(\kappa + 1)}. \tag{9}$$

At the remote place, the complex potentials shown by Eq. (8) can be rewritten in the form

$$\phi_{(\alpha)}(z) = F\left(\ln z - \sum_{k=1}^{\infty} \frac{1}{k} \left(\frac{t}{z} \right)^k \right), \quad \psi_{(\alpha)}(z) = -\kappa \bar{F} \left(\ln z - \sum_{k=1}^{\infty} \frac{1}{k} \left(\frac{t}{z} \right)^k \right) - \frac{F\bar{t}}{z} \left(\sum_{k=0}^{\infty} \left(\frac{t}{z} \right)^k \right). \tag{10}$$

Clearly, the expression shown by Eqs. (8) or (10) belongs to the pure deformation representation of the stress field, since each term in Eq. (8) has its stress distribution in the elastic medium.

Comparing Eq. (4) with Eq. (8), we see that $a_0 = 0$, $b_0 = 0$ in the α-field. Substituting this result ($a_0 = 0$, $b_0 = 0$) into Eq. (7) yields

$$D_{(\mathrm{CR})} = \oint_{(\mathrm{CR})} \left(u_{i(\alpha)} \sigma_{ij(\beta)} - u_{i(\beta)} \sigma_{ij(\alpha)} \right) n_j \mathrm{d}s = 0. \tag{11}$$

In addition, if the concentrated forces (P_x, P_y) are applied at the point $z = t$ (Fig. 1a), the relevant complex potentials can be expressed in an alternative form

$$\phi_{(\alpha)}(z) = F \ln(z - t), \quad \psi_{(\alpha)}(z) = -\kappa \bar{F} \ln (z - t) - \frac{F\bar{t}}{z - t} + \bar{F}, \tag{12}$$

where F has been defined in Eq. (9). Clearly, the complex potentials shown by Eqs. (8) and (12) have a difference $\bar{F}$ in the complex potential $\psi_{(\alpha)}(z)$.

At the remote place, the complex potentials shown by Eq. (12) can be rewritten in the form

$$\begin{aligned} \phi_{(\alpha)}(z) &= F \left(\ln z - \sum_{k=1}^{\infty} \frac{1}{k} \left(\frac{t}{z} \right)^k \right), \\ \psi_{(\alpha)}(z) &= -\kappa \bar{F} \left(\ln z - \sum_{k=1}^{\infty} \frac{1}{k} \left(\frac{t}{z} \right)^k \right) - \frac{F\bar{t}}{z} \left(\sum_{k=0}^{\infty} \left(\frac{t}{z} \right)^k \right) + \bar{F}. \end{aligned} \tag{13}$$

Comparing Eq. (4) with Eq. (13), we see that $a_0 = 0$, $b_0 = \bar{F}$ in the α-field. Substituting this result ($a_0 = 0$, $b_0 = \bar{F}$) into Eq. (7) yields

$$D_{(\mathrm{CR})} = \oint_{(\mathrm{CR})} \left(u_{i(\alpha)} \sigma_{ij(\beta)} - u_{i(\beta)} \sigma_{ij(\alpha)} \right) n_j \mathrm{d}s = -\frac{\pi(\kappa + 1)}{G} Re[b_0 E_2] \neq 0. \tag{14}$$

However, if the β-field is a stress field such that the forces applied on the finite portion are in equilibrium, then, we have $E_2 = 0$, $F_2 = 0$. Substituting this result ($E_2 = 0$) into Eq. (14) yields

$$D_{(\mathrm{CR})} = \oint_{(\mathrm{CR})} \left(u_{i(\alpha)} \sigma_{ij(\beta)} - u_{i(\beta)} \sigma_{ij(\alpha)} \right) n_j \mathrm{d}s = 0. \tag{15}$$

2.2 A new kernel $U_{ij}^{*1}(\xi, x)$ with the relevant formulation of BIE

Without losing generality, we can introduce the BIE for the region between the elliptic contour Γ and a large circle CR (Fig. 1b). The observation point ξ is assumed on the elliptic contour $\xi \in \Gamma$.

If we use the complex potentials (or the fundamental solution) shown by Eq. (8), for the plane strain case, the suggested BIE can be written as follows [3]:

$$\frac{1}{2} u_i(\xi) + \int_{\Gamma} P_{ij}^*(\xi, x) u_j(x) \mathrm{d}s(x) = \int_{\Gamma} U_{ij}^{*1}(\xi, x) p_j(x) \mathrm{d}s(x) + D_{i(\mathrm{CR})}^{*1}(\xi), \quad (i = 1, 2, \xi \in \Gamma), \tag{16}$$

where $D_{i(\mathrm{CR})}^{*1}(\xi)$ is an MWDI on a large circle and is defined by

$$D_{i(\mathrm{CR})}^{*1}(\xi) = -\int_{\mathrm{CR}} P_{ij}^*(\xi, x) u_j(x) \mathrm{d}s(x) + \int_{\mathrm{CR}} U_{ij}^{*1}(\xi, x) p_j(x) \mathrm{d}s(x), \quad (i = 1, 2, \xi \in \Gamma) \tag{17}$$

and the kernel $P_{ij}^*(\xi, x)$ is defined by [3]

$$P_{ij}^*(\xi, x) = -\frac{1}{4\pi(1 - \upsilon)} \frac{1}{r} \left\{ (r_{,1} n_1 + r_{,2} n_2)((1 - 2\upsilon)\delta_{ij} + 2 r_{,i} r_{,j}) + (1 - 2\upsilon)(n_i r_{,j} - n_j r_{,i}) \right\}, \tag{18}$$

where Kronecker deltas δ_{ij} are defined as $\delta_{ij} = 1$ for $i = j$, $\delta_{ij} = 0$ for $i \neq j$, and

$$r_{,1} = \frac{x_1 - \xi_1}{r} = \cos\ \alpha, \quad r_{,2} = \frac{x_2 - \xi_2}{r} = \sin\alpha,$$
$$n_1 = -\sin\beta, \quad n_2 = \cos\beta, \tag{19}$$

where the angles α and β are indicated in Fig. 1.

The kernel $U_{ij}^{*1}(\xi, x)$ can be obtained in the following manner. By taking the following steps: (a) $P_x = 1$, and $P_y = 0$ (or $P_x = 0$, $P_y = 1$) in Eqs. (8), (9), and (b) letting the point t approach the boundary point ξ (Fig. 1a, b) and letting the point z approach the boundary point x (here x denotes a point in the kernel $U_{ij}^{*1}(\xi, x)$) (Fig. 1a), from Eq. (3) we can obtain two displacements $U_{11}^{*1}(\xi, x)$, $U_{12}^{*1}(\xi, x)$ (or $U_{21}^{*1}(\xi, x)$, $U_{22}^{*1}(\xi, x)$). Finally, the kernel $U_{ij}^{*1}(\xi, x)$ is obtained as

$$U_{ij}^{*1}(\xi, x) = \frac{1}{8\pi(1-v)G}\left\{-(3-4v)\ln(r)\delta_{ij} + r_{,i}r_{,j} - 0.5\delta_{ij}\right\}. \tag{20}$$

In fact, the integral $D_{i(\mathrm{CR})}^{*1}(\xi)$ shown by Eq. (17) is an MWDI defined by Eq. (7). In this case, the complex potentials for driving $U_{ij}^{*1}(\xi, x)$ are shown by Eq. (8), and Eq. (11) is valid (or $D_{(\mathrm{CR})} = 0$) in this case. Therefore, from Eq. (11) we have

$$D_{i(\mathrm{CR})}^{*1}(\xi) = 0, \quad (i = 1, 2, \xi \in \Gamma). \tag{21}$$

Alternatively speaking, if the complex potentials shown by Eq. (8) are used, or the kernel $U_{ij}^{*1}(\xi, x)$ shown by Eq. (20) is used, we can drop the term $D_{i(\mathrm{CR})}^{*1}(\xi)$ in Eq. (16), and the following BIE is obtained:

$$\frac{1}{2}u_i(\xi) + \int_\Gamma P_{ij}^*(\xi, x)u_j(x)\mathrm{d}s(x) = \int_\Gamma U_{ij}^{*1}(\xi, x)p_j(x)\mathrm{d}s(x), \quad (i = 1, 2, \xi \in \Gamma). \tag{22}$$

It is emphasized here that the BIE shown by (22) can even be used *for arbitrary loading case*, when the applied loadings on the contour are not in equilibrium.

2.3 The usual kernel $U_{ij}^{*2}(\xi, x)$ with the relevant formulation of BIE

The usual kernel $U_{ij}^{*2}(\xi, x)$ and the relevant BIE was introduced previously [3]. However, we prefer to introduce the kernel and the relevant BIE in the following manner.

Similar to the abovementioned case, we use the complex potentials (or the fundamental solution) shown by Eq. (12), which are different from the complex potentials shown by Eq. (8) by a constant $\bar{F}$ in the complex potential $\psi_{(\alpha)}(z)$.

As before, we can obtain the BIE as follows [3]:

$$\frac{1}{2}u_i(\xi) + \int_\Gamma P_{ij}^*(\xi, x)u_j(x)\mathrm{d}s(x) = \int_\Gamma U_{ij}^{*2}(\xi, x)p_j(x)\mathrm{d}s(x) + D_{i(\mathrm{CR})}^{*2}(\xi), \quad (i = 1, 2, \xi \in \Gamma) \tag{23}$$

where $D_{i(\mathrm{CR})}^{*2}(\xi)$ is an MWDI on a large circle and is defined by

$$D_{i(\mathrm{CR})}^{*2}(\xi) = -\int_{\mathrm{CR}} P_{ij}^*(\xi, x)u_j(x)\mathrm{d}s(x) + \int_{\mathrm{CR}} U_{ij}^{*2}(\xi, x)p_j(x)\mathrm{d}s(x), \quad (i = 1, 2, \xi \in \Gamma). \tag{24}$$

In Eq. (23), the kernel $P_{ij}^*(\xi, x)$ has been defined in Eq. (18).

As in the case of using the kernel $U_{ij}^{*1}(\xi, x)$, from the complex potentials shown by Eq. (12), we can obtain the kernel $U_{ij}^{*2}(\xi, x)$ as follows:

$$U_{ij}^{*2}(\xi, x) = \frac{1}{8\pi(1-v)G}\left\{-(3-4v)\ln(r)\delta_{ij} + r_{,i}r_{,j}\right\}. \tag{25}$$

Clearly, the kernels shown by Eqs. (20) and (25) have a difference of $-0.5\delta_{ij}/(8\pi(1-v)G)$.

In fact, the integral $D^{*2}_{i(\mathrm{CR})}(\xi)$ shown by Eq. (25) is an MWDI defined by Eq. (7). In this case of the nonequilibrated loadings on the contour, the complex potentials for driving $U^{*2}_{ij}(\xi, x)$ are shown by Eq. (12), and Eq. (14) is valid in this case ($D_{(\mathrm{CR})} \neq 0$). Therefore, from Eq. (14), in the case of nonequilibrated loadings on the contour, we have

$$D^{*2}_{i(\mathrm{CR})}(\xi) \neq 0, \quad (i = 1, 2, \xi \in \Gamma). \tag{26}$$

Alternatively speaking, in the case of nonequilibrated loadings on the contour, if the complex potentials shown by Eq. (12) are used, or the kernel $U^{*2}_{ij}(\xi, x)$ shown by Eq. (25) is used, we cannot drop the term $D^{*2}_{i(\mathrm{CR})}(\xi)$ in Eq. (23), and the BIE shown by Eq. (23) cannot be reduced further.

In addition, in the case of equilibrated loadings on the contour, Eq. (15) is valid ($D_{(\mathrm{CR})} = 0$). Therefore, from Eq. (15), in case of equilibrated loadings on the contour, we have

$$D^{*2}_{i(\mathrm{CR})}(\xi) = 0, \quad (i = 1, 2, \xi \in \Gamma). \tag{27}$$

Alternatively speaking, in the case of equilibrated loadings on the contour, if the complex potentials shown by Eq. (12) are used, or the kernel $U^{*2}_{ij}(\xi, x)$ shown by Eq. (25) is used, we can drop the term $D^{*2}_{i(\mathrm{CR})}(\xi)$in Eq. (23), and the following BIE is obtained

$$\frac{1}{2}u_i(\xi) + \int_\Gamma P^*_{ij}(\xi, x)u_j(x)\mathrm{d}s(x) = \int_\Gamma U^{*2}_{ij}(\xi, x)p_j(x)\mathrm{d}s(x), \quad (i = 1, 2, \xi \in \Gamma). \tag{28}$$

It is emphasized here that the BIE shown by (28) can only be used *for the case of equilibrated loadings the on contour*.

In addition, for the case of the loadings $p_j(x)$ in equilibrium, the results from the usage of the kernel $U^{*1}_{ij}(\xi, x)$ or $U^{*2}_{ij}(\xi, x)$ are equivalent. In fact, from subtraction of the right hand terms in Eqs. (22) and (28), we can find

$$\int_\Gamma \left(U^{*1}_{ij}(\xi, x) - U^{*2}_{ij}(\xi, x)\right) p_j(x)\mathrm{d}s(x) = -\frac{1}{16\pi(1-\nu)G}\int_\Gamma \delta_{ij}p_j(x)\mathrm{d}s(x) = 0. \tag{29}$$

Therefore, the mentioned statement is proved.

3 Numerical examinations for the usage of two kernels $U^{*1}_{ij}(\xi, x)$ and $U^{*2}_{ij}(\xi, x)$ in the exterior Neumann problem

In the Neumann problem, the boundary tractions $\tilde{p}_j(x)(j = 1, 2)$ are given beforehand. Therefore, in the case of using the kernel $U^{*1}_{ij}(\xi, x)$, from Eq. (22), we can obtain the following BIE:

$$\frac{1}{2}u_i(\xi) + \int_\Gamma P^*_{ij}(\xi, x)u_j(x)\mathrm{d}s(x) = g_i(\xi), \quad (i = 1, 2, \xi \in \Gamma), \tag{30}$$

where

$$g_i(\xi) = \int_\Gamma U^{*1}_{ij}(\xi, x)\tilde{p}_j(x)\mathrm{d}s(x), \quad (i = 1, 2, \xi \in \Gamma). \tag{31}$$

In Eq. (31), $\tilde{p}_j(x)$ $(j = 1, 2)$ are the boundary tractions that are given beforehand.

Similarly, in the case of using the kernel $U^{*2}_{ij}(\xi, x)$, from Eq. (28), we can obtain the following BIE:

$$\frac{1}{2}u_i(\xi) + \int_\Gamma P^*_{ij}(\xi, x)u_j(x)\mathrm{d}s(x) = h_i(\xi), \quad (i = 1, 2, \xi \in \Gamma), \tag{32}$$

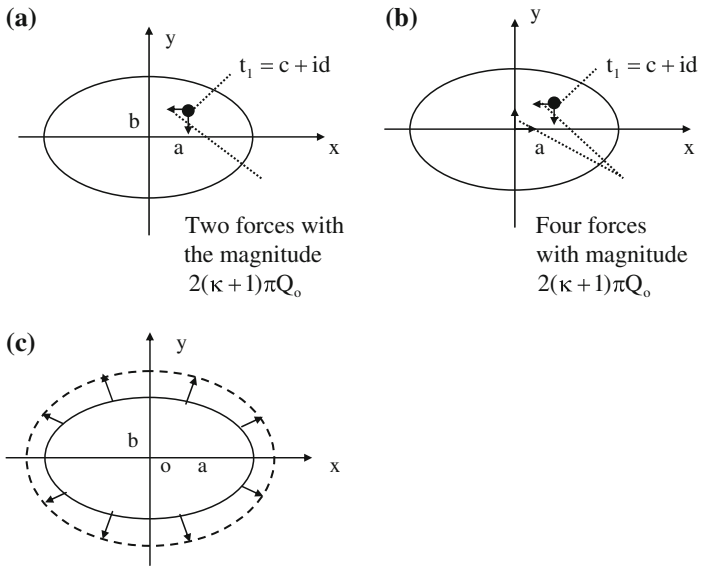

Fig. 2 **a** A nonequilibrated loading applied on the elliptic contour. **b** An equilibrated loading with moment applied on the elliptic contour. **c** An elliptic contour with symmetric deformation

where

$$h_i(\xi) = \int_\Gamma U_{ij}^{*2}(\xi, x)\tilde{p}_j(x)\mathrm{d}s(x), \quad (i = 1, 2, \xi \in \Gamma). \tag{33}$$

In Eq. (33), $\tilde{p}_j(x)$ $(j = 1, 2)$ are the boundary tractions that are given beforehand.

The abovementioned results from theoretical analysis can be examined by the following concrete examples. In the examples, the ellipse has a major half-axis a and minor half-axis b (Fig. 2a). In computation, the plane strain condition and $\nu = 0.3$ are assumed. The elliptic contour is divided into 120 intervals. For the BIE solution, the constant displacement and traction are assumed for each interval.

In the first example, we propose the following complex potentials (Fig. 2a):

$$\phi(z) = Q_o(1 + \mathrm{i})\ln(z - t_1), \quad \psi(z) = -\kappa Q_o(1 - \mathrm{i})\ln(z - t_1), \quad t_1 = c + \mathrm{i}d, \tag{34}$$

where Q_o is a given loading. The loadings on the elliptic contour can be derived from the assumed complex potentials (34) and Eq. (1). Those loadings result in the resultant forces $2\pi(\kappa + 1)Q_o$ as indicated in Fig. 2a. Clearly, those loadings are not in equilibrium.

The applied tractions on the contour, or $\tilde{p}_j$ $(j = 1, 2)$ are computed from the complex potentials shown by Eq. (34), and the tractions $\tilde{p}_j$ $(j = 1, 2)$ are substituted into the right-hand term of Eq. (31) (or (33)). Standard numerical technique is used to solve Eq. (30) (or (32)), and the boundary displacements u_j $(j = 1, 2)$ can be evaluated immediately. In computation, $a = 3, b/a = 0.5, c/a = 0.25$ and $d/b = 0.25$ are assumed. The calculated boundary displacements by using the kernels $U_{ij}^{*1}(\xi, x)$or $U_{ij}^{*2}(\xi, x)$, and those from the exact solution are expressed by the same equation:

$$u_1 = \frac{Q_o}{2Ga}F_1(\theta), \quad u_2 = \frac{Q_o}{2Ga}F_2(\theta) \quad (\text{at the point } x = a\cos\theta, y = b\sin\theta). \tag{35}$$

The computed results for $F_1(\theta)$ and $F_2(\theta)$ are plotted in Fig. 3. It is found from Fig. 3 that the computed results for $F_1(\theta)$ and $F_2(\theta)$ from the usage of the kernel $U_{ij}^{*1}(\xi, x)$ are very accurate, and coincide with the results from the exact solution. However, the computed results for $F_1(\theta)$ and $F_2(\theta)$ from the usage of the kernel $U_{ij}^{*2}(\xi, x)$ show a large difference from those of the exact solution. Therefore, from the computed results in Fig. 3, it is proved that the BIE based on the usage of the kernel $U_{ij}^{*2}(\xi, x)$ cannot be used in the case of nonequilibrated loading on the contour.

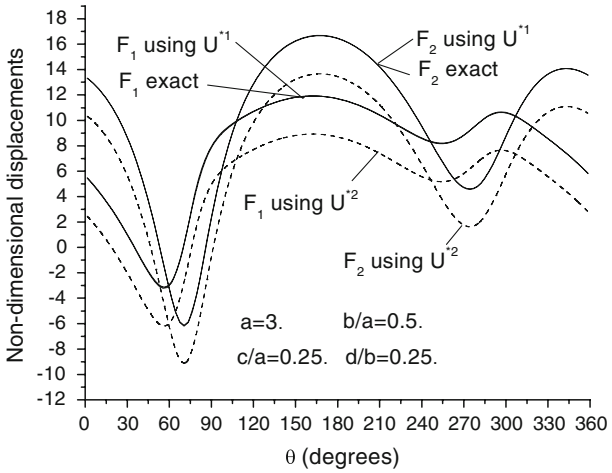

Fig. 3 Nondimensional displacements $F_1(\theta)$, $F_2(\theta)$ for an exterior Neumann problem with nonequilibrated loadings on the contour with the usage of the kernels $U_{ij}^{*1}(\xi, x)$, $U_{ij}^{*2}(\xi, x)$ and the exact solution (see Fig. 2a and Eq. (35))

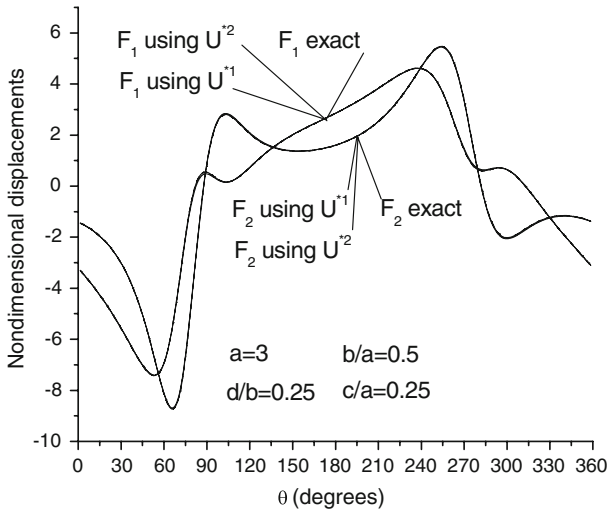

Fig. 4 Nondimensional displacements $F_1(\theta)$, $F_2(\theta)$ for an exterior Neumann problem with equilibrated loadings on the contour with the usage of the kernels $U_{ij}^{*1}(\xi, x)$, $U_{ij}^{*2}(\xi, x)$ and the exact solution (see Fig. 2b and Eq. (35))

In the second example, we propose the following complex potentials (Fig. 2b):

$$\phi(z) = Q_o(1+\mathrm{i})(\ln(z-t_1) - \ln z), \quad \psi(z) = -\kappa Q_o(1-\mathrm{i})(\ln(z-t_1) - \ln z), \quad (\text{where } t_1 = c + \mathrm{i}d), \tag{36}$$

where Q_o is a given loading. The loadings on the elliptic contour can be derived from the assumed complex potentials (36) and Eq. (1). Those loadings result in a moment as indicated in Fig. 2b. Thus, those loadings are equilibrated in forces, but not in moment.

In the second example, the computation condition is same as in the first example. As before, the calculated boundary displacements by using the kernels $U_{ij}^{*1}(\xi, x)$ or $U_{ij}^{*2}(\xi, x)$ and those from the exact solution are expressed by the same Eq. (35).

The computed results for $F_1(\theta)$ and $F_2(\theta)$ are plotted in Fig. 4. It is found from Fig. 4 that the computed results for $F_1(\theta)$ and $F_2(\theta)$ from the usage of the kernels $U_{ij}^{*1}(\xi, x)$ and $U_{ij}^{*2}(\xi, x)$ and the exact results directly from the complex potentials (36) are the same. Therefore, from the computed results in Fig. 4, we prove that the BIE based on the usage of the kernels $U_{ij}^{*1}(\xi, x)$ or $U_{ij}^{*2}(\xi, x)$ can be used for the case of equilibrated loading on the contour.

A possibility for reducing the original boundary value problem is introduced below. It is assumed that there are some nonequilibrated loadings applied on the contour. In this case, one needs to introduce a particular problem such that the particular problem has the same nonequilibrated loadings as in the original problem. After introducing the particular problem, the original problem can be reduced to a modified problem with equilibrated loadings applied on the contour. Clearly, in the modified problem, one can use the kernel $U_{ij}^{*2}(\xi, x)$. Clearly, this technique can only be used for the case of the exterior Neumann problem. In the exterior Dirichlet problem, this technique is no longer valid, which will be described in detail below.

4 Numerical examinations for the usage of two kernels $U_{ij}^{*1}(\xi, x)$ and $U_{ij}^{*2}(\xi, x)$ in the exterior Dirichlet problem

As similar idea as mentioned in the previous section can be developed to the exterior Dirichlet problem. In the Dirichlet problem, the boundary displacements $\tilde{u}_j(x)$ $(j = 1, 2)$ are given beforehand. Therefore, in the case of using the kernel $U_{ij}^{*1}(\xi, x)$, from Eq. (22) we can obtain the following BIE:

$$\int_{\Gamma} U_{ij}^{*1}(\xi, x) p_j(x) \mathrm{d}s(x) = g_i(\xi), \quad (i = 1, 2, \xi \in \Gamma), \tag{37}$$

where

$$g_i(\xi) = \frac{1}{2}\tilde{u}_i(\xi) + \int_{\Gamma} P_{ij}^{*}(\xi, x)\tilde{u}_j(x)\mathrm{d}s(x), \quad (i = 1, 2, \xi \in \Gamma). \tag{38}$$

In Eq. (38), $\tilde{u}_i(\xi)(i = 1, 2)$ and $\tilde{u}_j(x)$ $(j = 1, 2)$ are the boundary displacements that are given beforehand.

Similarly, in the case of using the kernel $U_{ij}^{*2}(\xi, x)$, from Eq. (28) we can obtain the following BIE:

$$\int_{\Gamma} U_{ij}^{*2}(\xi, x) p_j(x) \mathrm{d}s(x) = h_i(\xi), \quad (i = 1, 2, \xi \in \Gamma), \tag{39}$$

where

$$h_i(\xi) = \frac{1}{2}\tilde{u}_i(\xi) + \int_{\Gamma} P_{ij}^{*}(\xi, x)\tilde{u}_j(x)\mathrm{d}s(x), \quad (i = 1, 2, \xi \in \Gamma). \tag{40}$$

In Eq. (40), $\tilde{u}_i(\xi)(i = 1, 2)$ and $\tilde{u}_j(x)$ $(j = 1, 2)$ are the boundary displacements that are given beforehand.

The abovementioned results from theoretical analysis can be examined by the following concrete examples. All the computation conditions are the same as in the previous section.

In the first example, we propose the complex potentials defined by Eq. (34). As mentioned previously, the loadings applied on the contour result in the resultant forces $2\pi(\kappa + 1)Q_o$ as indicated in Fig. 2a. Thus, those loadings are not in equilibrium.

The displacements applied on the contour, or $\tilde{u}_j$ $(j = 1, 2)$, are computed from the complex potentials shown by Eqs. (3) and (34), and the obtained tractions $\tilde{u}_j$ $(j = 1, 2)$ are substituted into the right-hand term of Eq. (38) (or (40)). Standard numerical technique is used to solve Eq. (37) (or (39)), and the boundary tractions p_j $(j = 1, 2)$ can be evaluated immediately. In the computation, $a = 3$, $b/a = 0.5$, $c/a = 0.25$ and $d/b = 0.25$ are assumed. The computed boundary tractions by using the kernels $U_{ij}^{*1}(\xi, x)$ or $U_{ij}^{*2}(\xi, x)$, and those from the exact solution are expressed by the same equation

$$p_1 = \frac{Q_o}{a}G_1(\theta), \quad p_2 = \frac{Q_o}{a}G_2(\theta) \quad (\text{at the point } x = a\cos\theta, y = b\sin\theta). \tag{41}$$

The computed results for $G_1(\theta)$ and $G_2(\theta)$ are plotted in Fig. 5. It is found from Fig. 5 that the computed results for $G_1(\theta)$ and $G_2(\theta)$ from the usage of the kernel $U_{ij}^{*1}(\xi, x)$ are very accurate, coinciding with the results from the exact solution. However, the computed results for $G_1(\theta)$ and $G_2(\theta)$ from the usage of the kernel $U_{ij}^{*2}(\xi, x)$ show a large difference from those of the exact solution. Therefore, from the computed results

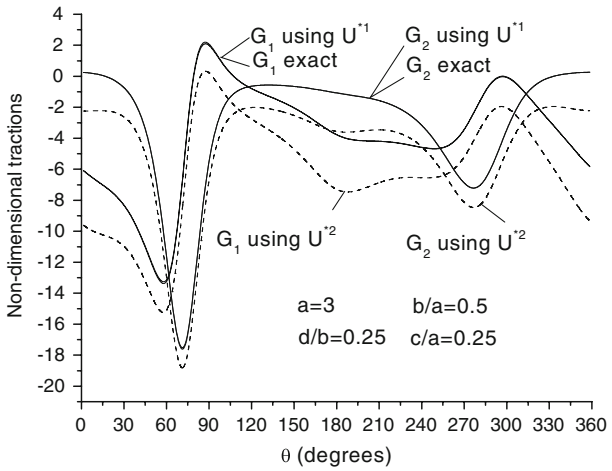

Fig. 5 Nondimensional tractions $G_1(\theta)$, $G_2(\theta)$ for an exterior Dirichlet problem with nonequilibrated loadings on the contour with the usage of the kernels $U_{ij}^{*1}(\xi, x)$, $U_{ij}^{*2}(\xi, x)$and the exact solution (see Fig. 2a and Eq. (41))

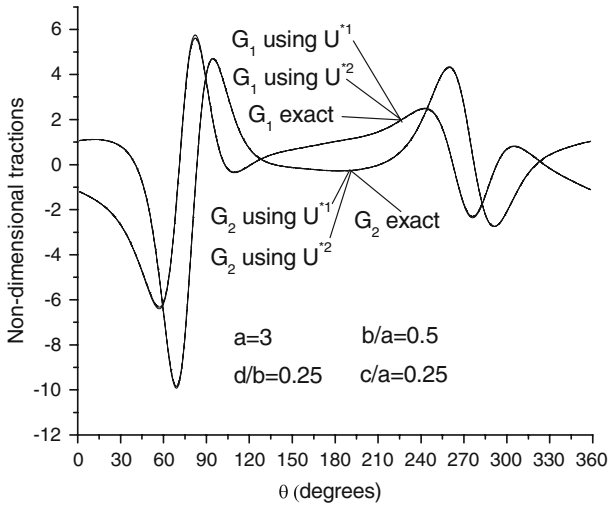

Fig. 6 Nondimensional tractions $G_1(\theta)$, $G_2(\theta)$ for an exterior Dirichlet problem with equilibrated loadings on the contour with the usage of the kernels $U_{ij}^{*1}(\xi, x)$, $U_{ij}^{*2}(\xi, x)$ and the exact solution (see Fig. 2b and Eq. (41))

in Fig. 5, we prove that the BIE based on the usage of the kernel $U_{ij}^{*2}(\xi, x)$ cannot be used for the case of the exterior Dirichlet problem in general.

In the second example, we propose the complex potentials defined by Eq. (36). The displacements on the elliptic contour can be derived from the assumed complex potentials (36) and Eq. (4). Those loadings result in a moment as indicated in Fig. 2b. Thus, those loadings are equilibrated in forces, but not in moment.

In the second example, the computation condition is same as in the first example. As before, the calculated boundary tractions by using the kernels $U_{ij}^{*1}(\xi, x)$ or $U_{ij}^{*2}(\xi, x)$, and those from the exact solution are expressed by the same Eq. (41).

The computed results for $G_1(\theta)$ and $G_2(\theta)$ are plotted in Fig. 6. It is found from Fig. 6 that the computed results for $G_1(\theta)$ and $G_2(\theta)$ from the usage of the kernels $U_{ij}^{*1}(\xi, x)$ and $U_{ij}^{*2}(\xi, x)$ and the exact results directly from the complex potentials (36) are the same. Therefore, from the computed results in Fig. 6, we prove that the BIE based on the usage of the kernels $U_{ij}^{*1}(\xi, x)$ or $U_{ij}^{*2}(\xi, x)$ can be used for the case of equilibrated loading on the contour.

As mentioned previously, the displacements on the contour in the exterior Dirichlet problem are given beforehand. However, it is impossible to judge whether the assumed boundary displacements cause the

equilibrated loadings on the contour or not. Therefore, one must use the BIE based on the kernel $U_{ij}^{*1}(\xi, x)$ to solve the exterior Dirichlet problem in general.

In the elliptic contour with a symmetric deformation (Fig. 2c), the relevant tractions applied on the contour must be in equilibrium. Only for this case, the BIE based on the kernel $U_{ij}^{*2}(\xi, x)$ can be used for the exterior Dirichlet problem.

5 A particular exterior Dirichet problem for an infinite plate with inclusion

It has been proved that if the forces applied on the elliptic contour result in a resultant force, we have to use the BIE shown by Eq. (22). This is universal. However, when the plate was inserted by an inclusion and the inclusion has a deformation and some loading on it, the solution is more complicated. This topic will be studied below.

5.1 Formulation of the problem

Previously, we have introduced the following BIE for the exterior Dirichlet problem:

$$\int_{\Gamma} U_{ij}^{*1}(\xi, x) p_j(x) \mathrm{d}s(x) = g_i(\xi), \quad (i = 1, 2, \xi \in \Gamma), \tag{37}$$

where

$$g_i(\xi) = \frac{1}{2}\tilde{u}_i(\xi) + \int_{\Gamma} P_{ij}^{*}(\xi, x)\tilde{u}_j(x)\mathrm{d}s(x), \quad (i = 1, 2, \xi \in \Gamma). \tag{38}$$

In Eq. (38), $\tilde{u}_i(\xi)(i = 1, 2)$ and $\tilde{u}_j(x)$ $(j = 1, 2)$ are the boundary displacements, which are given beforehand. Equations (37) and (38) will also be used in the formulation of a particular exterior Dirichlet problem.

It is assumed that an inclusion is inserted in the infinite plate, and the inclusion has a deformation $u + \mathrm{i}v = d_1(t) + \mathrm{i}d_2(t)(t \in \Gamma)$ (Fig. 7a). The deformation is called the initial deformation hereafter. On the other hand, there are some forces Q_x, Q_y and moment M_o applied on the inclusion (Fig. 7a). In this case, in accordance with the applied forces and moment on the inclusion, there must be an additional rigid translation and rotation for the inclusion. Therefore, the displacement boundary condition will be

$$\begin{Bmatrix} \tilde{u}_1 \\ \tilde{u}_2 \end{Bmatrix} = \begin{Bmatrix} d_1 \\ d_2 \end{Bmatrix} + \alpha_1 \begin{Bmatrix} 1 \\ 0 \end{Bmatrix} + \alpha_2 \begin{Bmatrix} 0 \\ 1 \end{Bmatrix} + \alpha_3 \begin{Bmatrix} -y_t \\ x_t \end{Bmatrix}, \quad (t = x_t + \mathrm{i}y_t \in \Gamma). \tag{42}$$

In the right-hand side of Eq. (42), the first term denotes the initial deformation along the elliptic contour, the second and third terms represent a rigid translation of inclusion, and the fourth term represents a rigid rotation. The involved constants $\alpha_1, \alpha_2, \alpha_3$ can be determined by the condition that Q_x, Q_y and the moment M_o are applied on the inclusion.

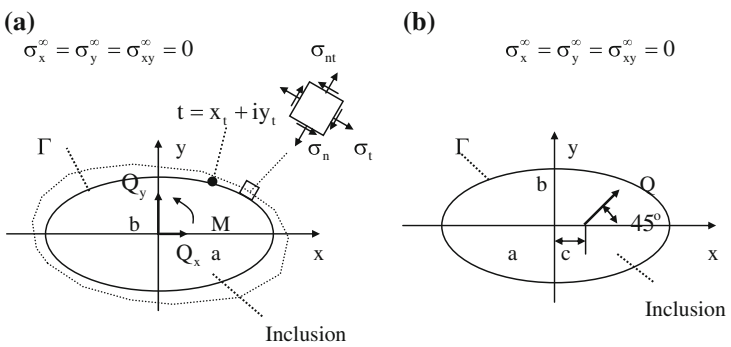

Fig. 7 **a** An inclusion with initial deformation and with the applied forces Q_x, Q_y and moment M_o. **b** An inclusion with the applied forces Q

Substituting Eq. (42) into (38) yields (see Appendix)

$$g_i(\xi) = G_i(\xi) + \sum_{k=1}^{3} \alpha_k b_i^{(k)}(\xi), \tag{43}$$

where

$$G_i(\xi) = \frac{1}{2} d_i(\xi) + \int_\Gamma P_{ij}^*(\xi, x) d_j(x) \mathrm{d}s(x), \tag{44}$$

$$\begin{Bmatrix} b_1^{(1)} \\ b_2^{(1)} \end{Bmatrix} = \begin{Bmatrix} 1 \\ 0 \end{Bmatrix}, \quad \begin{Bmatrix} b_1^{(2)} \\ b_2^{(2)} \end{Bmatrix} = \begin{Bmatrix} 0 \\ 1 \end{Bmatrix}, \quad \begin{Bmatrix} b_1^{(3)} \\ b_2^{(3)} \end{Bmatrix} = \begin{Bmatrix} -y_t \\ x_t \end{Bmatrix}. \tag{45}$$

Alternatively, the BIE shown by Eq. (37) can be rewritten as

$$\int_\Gamma U_{ij}^{*1}(\xi, x) p_j(x) \mathrm{d}s(x) = G_i(\xi) + \sum_{k=1}^{3} \alpha_k b_i^{(k)}(\xi), \quad (i = 1, 2, \xi \in \Gamma). \tag{46}$$

The proposed problem can be solved by unit unknown technique. In the solution, we can propose four BIEs and their solutions as follows:

$$\int_\Gamma U_{ij}^{*1}(\xi, x) p_j(x) \mathrm{d}s(x) = G_i(\xi), \quad (i = 1, 2, \xi \in \Gamma) \quad \text{with solutions } p_j^{(\mathrm{in})}(x) \ (j = 1, 2, x \in \Gamma), \tag{47}$$

$$\int_\Gamma U_{ij}^{*1}(\xi, x) p_j(x) \mathrm{d}s(x) = b_i^{(k)}(\xi), \quad (i = 1, 2, \xi \in \Gamma, k = 1, 2, 3)$$

$$\text{with solutions } p_j^{(k)}(x) \ (j = 1, 2, x \in \Gamma, k = 1, 2, 3). \tag{48}$$

In Eq. (47), the subscript "(in)" means that the solution is from the initial boundary displacements defined by Eq. (44).

For clarity, the obtained solutions $p_1^{(\mathrm{in})}, p_2^{(\mathrm{in})}, p_1^{(1)}, p_2^{(1)}, p_1^{(2)}, p_2^{(2)}, p_1^{(3)}, p_2^{(3)}$ are rewritten in the form $p_x^{(\mathrm{in})}, p_y^{(\mathrm{in})}, p_x^{(1)}, p_y^{(1)}, p_x^{(2)}, p_y^{(2)}, p_x^{(3)}, p_y^{(3)}$. Considering the following two points: (a) the whole problem is a linear superposition of abovementioned four particular boundary value problems, and (b) the forces and the moment applied on the inclusion are Q_x, Q_y, M_o, respectively, which in turn are the forces applied on the contour from the inserted inclusion; considering these, we will obtain

$$\begin{aligned}
&\alpha_1 \int_\Gamma p_x^{(1)}(s) \mathrm{d}s + \alpha_2 \int_\Gamma p_x^{(2)}(s) \mathrm{d}s + \alpha_3 \int_\Gamma p_x^{(3)}(s) \mathrm{d}s + \int_\Gamma p_x^{(\mathrm{in})}(s) \mathrm{d}s = Q_x, \\
&\alpha_1 \int_\Gamma p_y^{(1)}(s) \mathrm{d}s + \alpha_2 \int_\Gamma p_y^{(2)}(s) \mathrm{d}s + \alpha_3 \int_\Gamma p_y^{(3)}(s) \mathrm{d}s + \int_\Gamma p_y^{(\mathrm{in})}(s) \mathrm{d}s = Q_y, \\
&\alpha_1 \int_\Gamma \left(x_t p_y^{(1)}(s) - y_t p_x^{(1)}(s) \right) \mathrm{d}s + \alpha_2 \int_\Gamma \left(x_t p_y^{(2)}(s) - y_t p_x^{(2)}(s) \right) \mathrm{d}s \\
&\quad + \alpha_3 \int_\Gamma \left(x_t p_y^{(3)}(s) - y_t p_x^{(3)}(s) \right) \mathrm{d}s + \int_\Gamma \left(x_t p_y^{(\mathrm{in})}(s) - y_t p_x^{(\mathrm{in})}(s) \right) \mathrm{d}s = M_o.
\end{aligned} \tag{49}$$

From the algebraic equation (49), the undetermined constants $\alpha_1, \alpha_2, \alpha_3$ can be evaluated. Further, the final solution is obtained.

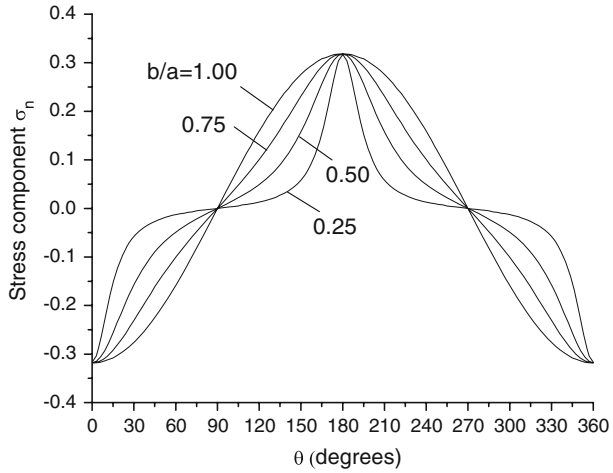

Fig. 8 Nondimensional stress component σ_n along the elliptic contour for a concentrated force Q_x applied on the inclusion (see Fig. 7a and Eq. (50))

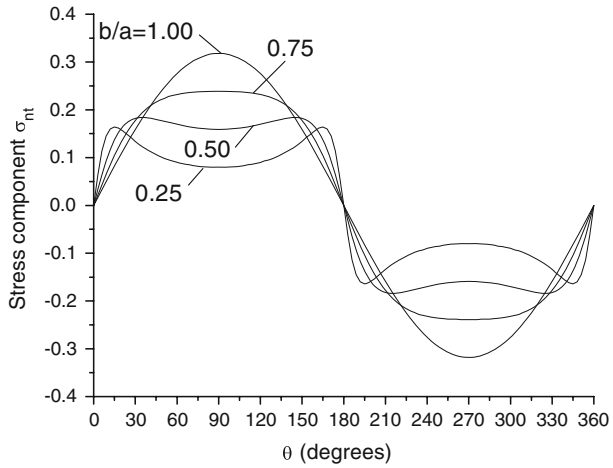

Fig. 9 Nondimensional stress component σ_{nt} along the elliptic contour for a concentrated force Q_x applied on the inclusion (see Fig. 7a and Eq. (50))

5.2 Numerical examples

In the computation, the elliptic contour is divided into 120 intervals. The constant displacement and traction are assumed for each interval. Standard numerical technique is used to solve the BIE shown by Eqs. (47) and (48) numerically.

Example 5.1 In the first example (Fig. 7a), we assume that the initial deformation vanishes, or $d_1(t)+\mathrm{i}d_2(t) = 0(t = x_t+\mathrm{i}y_t \in \Gamma)$, and the loading is Q_x only. The calculated stresses at the point $(x_t = a\cos\theta,\ y_t = b\sin\theta)$ along the elliptic contour are expressed as

$$\sigma_n = G_1(b/a,\theta)\frac{Q_x}{2b},\quad \sigma_{nt} = G_2(b/a,\theta)\frac{Q_x}{2b},\quad \sigma_t = G_3(b/a,\theta)\frac{Q_x}{2b}. \tag{50}$$

The calculated results for stresses $\sigma_n, \sigma_{nt}, \sigma_t$ for $b/a = 0.25, 0.50, 0.75$ and 1.00 are plotted in Figs. 8, 9 and 10, respectively. It is seen from these figures that the stress distributions are more smooth in the case of $b/a = 1.00$. In computation, the stress components σ_n and σ_{nt} can be obtained directly from the solution of the BIE, and the component σ_t can be evaluated for a technique suggested previously [13].

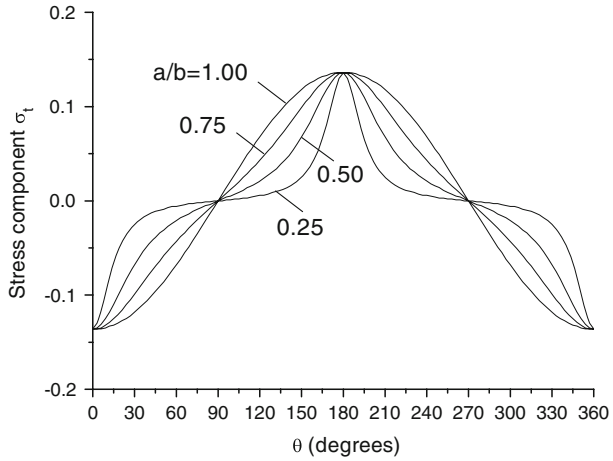

Fig. 10 Nondimensional stress component σ_t along the elliptic contour for a concentrated force Q_x applied on the inclusion (see Fig. 7a and Eq. (50))

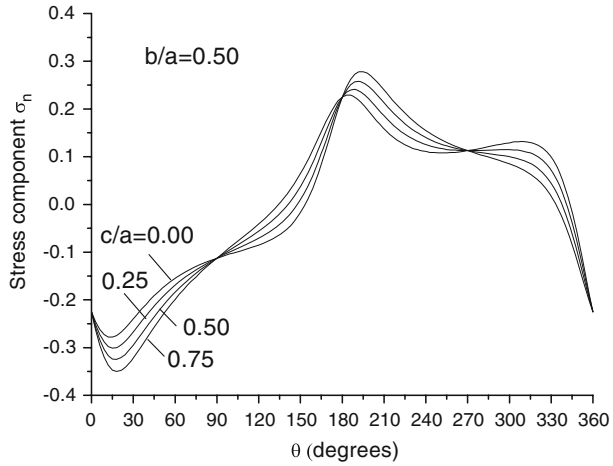

Fig. 11 Nondimensional stress component σ_n along the elliptic contour for a concentrated force Q applied on the inclusion (see Fig. 7b and Eq. (51))

Example 5.2 In the second example (Fig. 7b), we assume that the initial deformation vanishes, or $d_1(t) + \mathrm{i}d_2(t) = 0$ ($t = x_t + \mathrm{i}y_t \in \Gamma$), and the loading Q is applied at the location $(c, 0)$, which has an inclined angle of 45° with respect to the x-axis, $b/a = 0.50$ is assumed. The calculated stresses at the point ($x_t = a\cos\theta$, $y_t = b\sin\theta$) along the elliptic contour are expressed as

$$\sigma_n = H_1(c/a, \theta)\frac{Q}{2b}, \quad \sigma_{nt} = H_2(c/a, \theta)\frac{Q}{2b}, \quad \sigma_t = H_3(c/a, \theta)\frac{Q}{2b}. \tag{51}$$

The calculated results for stresses $\sigma_n, \sigma_{nt}, \sigma_t$ for $c/a = 0.00, 0.25, 0.50$ and 0.75 are plotted in Figs. 11, 12 and 13, respectively. From Fig. 11, we see that for $c/a = 0.75$ case, there is a peak stress for σ_n at $\theta = 18°$, $H_1 = -0.350$. The stress is the contact stress acting upon the elliptic contour from the inclusion.

Example 5.3 In the third example, we assume that the initial deformation is as follows (Fig. 7a):

$$d_1(t) + \mathrm{i}d_2(t) = u_o(1 + \sin\theta), \quad (t = x_t + \mathrm{i}y_t = a\cos\theta + \mathrm{i}b\sin\theta \in \Gamma). \tag{52}$$

No loading was applied on the inclusion, or $Q_x = Q_y = M_o = 0$. After some computation, the computed results are expressed as

$$\sigma_n = S_1(b/a, \theta)\frac{Eu_o}{a}, \quad \sigma_{nt} = S_2(b/a, \theta)\frac{Eu_o}{a}, \quad \sigma_t = S_3(b/a, \theta)\frac{Eu_o}{a}. \tag{53}$$

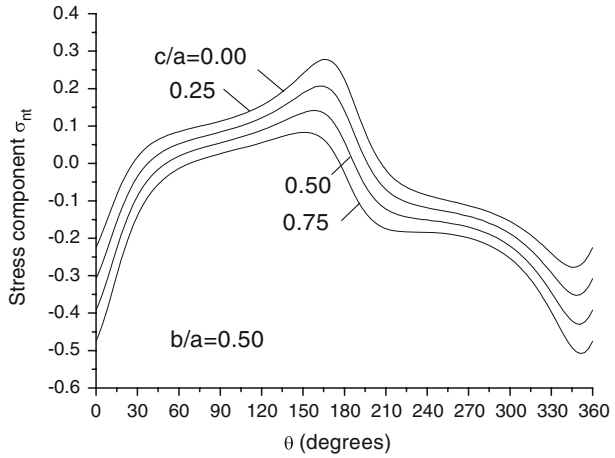

Fig. 12 Nondimensional stress component σ_{nt} along the elliptic contour for a concentrated force Q applied on the inclusion (see Fig. 7b and Eq. (51))

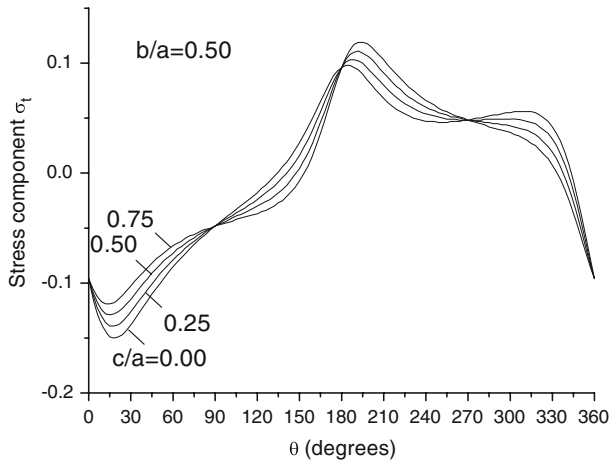

Fig. 13 Nondimensional stress component σ_t along the elliptic contour for a concentrated force Q applied on the inclusion (see Fig. 7b and Eq. (51))

The calculated results for stresses $\sigma_n, \sigma_{nt}, \sigma_t$ for $b/a = 0.25, 0.50, 0.75$ and 1.00 are plotted in Figs. 14, 15 and 16, respectively. From these figures, we see that for $b/a = 0.25$ case, there is a higher stress for σ_n andσ_t at $\theta = 15°$, $S_1 = -0.458$ and $S_3 = -2.389$. The stress component σ_n is the contact stress acting upon the elliptic contour from the inclusion.

6 Conclusions

The closed form solution for the MWDI shown in Eq. (7) provides a solid foundation in the present analysis [10]. In addition, the complex variable plays an important role in the derivation of the MWDI. If the solutions of the two stress fields are expressed in real variable, the mentioned MWDI is not easy to evaluate.

From the abovementioned theoretical analysis and the numerical examinations, we can get the following conclusions. The kernel $U_{ij}^{*1}(\xi, x)$ can be used for arbitrary loading on the contour. However, the $U_{ij}^{*2}(\xi, x)$ can only be used for the case in which the loadings on the contour are in equilibrium. This conclusion is particularly important for the case of the exterior Dirichlet problem. Since one cannot judge whether the boundary tractions caused by the given displacements are in equilibrium or not, one has to use the BIE with the kernel $U_{ij}^{*1}(\xi, x)$.

It is an effective way to examine a suggested BIE by using a known solution expressed in the complex potentials. In this case, since the solution is known beforehand, one can easily judge whether the formulation used in computation is correct or not.

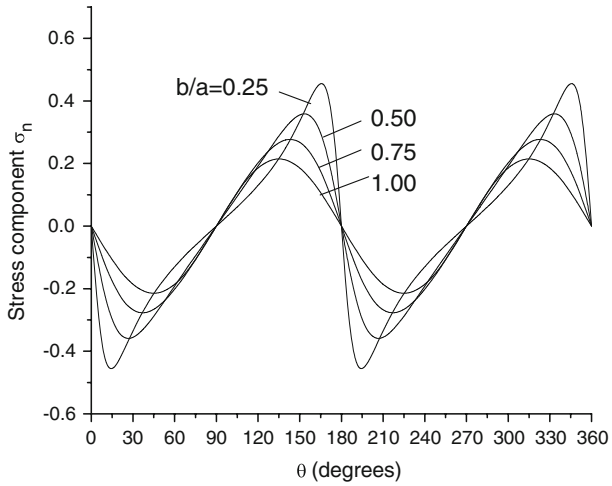

Fig. 14 Nondimensional stress component σ_n along the elliptic contour for assumed initial displacements on the contour (see Fig. 7a and Eqs. (52) and (53))

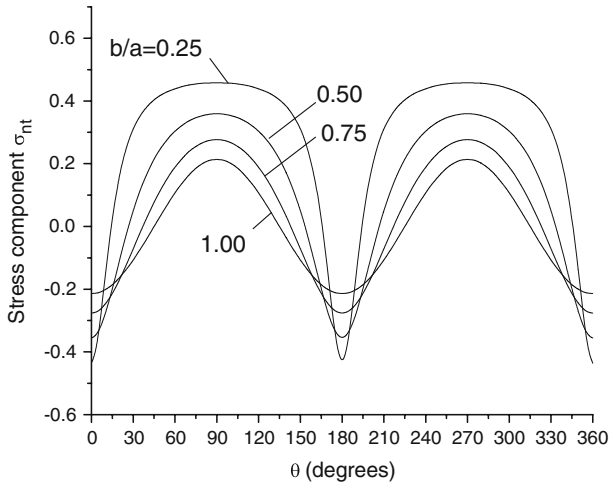

Fig. 15 Nondimensional stress component σ_{nt} along the elliptic contour for assumed initial displacements on the contour (see Fig. 7a and Eqs. (52) and (53))

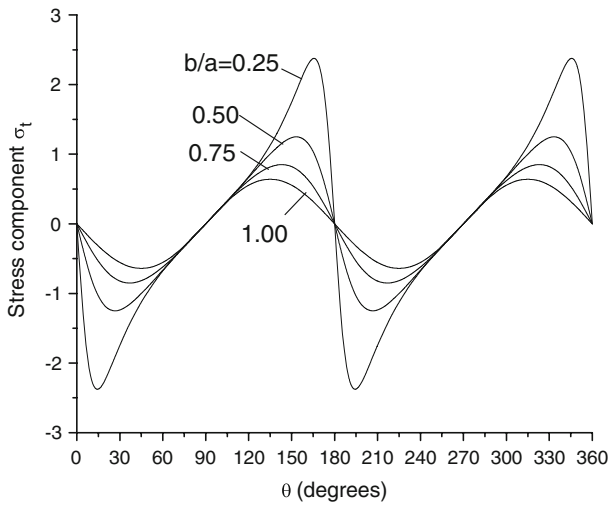

Fig. 16 Nondimensional stress component σ_t along the elliptic contour for assumed initial displacements on the contour (see Fig. 7a and Eqs. (52) and (53))

Appendix Derivation of an equality

In the exterior boundary value problem, from Eq. (38), the function $g_i(\xi)$ is defined as follows:

$$g_i(\xi) = \frac{1}{2}\tilde{u}_i(\xi) + \int_\Gamma P^*_{ij}(\xi, x)\tilde{u}_j(x)\mathrm{d}s(x), \quad (i = 1, 2, \xi \in \Gamma). \tag{A1}$$

Therefore, we can define an integration operator (with the subscript "ex")

$$\Pi_{(\mathrm{ex})}(\tilde{u}_j(x) \to g_i(\xi)) = \frac{1}{2}\tilde{u}_i(\xi) + \int_\Gamma P^*_{ij}(\xi, x)\tilde{u}_j(x)\mathrm{d}s(x), \quad (i = 1, 2\xi \in \Gamma). \tag{A2}$$

Note that, in the interior boundary value problem, the normal of the contour is oriented in the opposite direction to that of in the exterior problem. Thus, we can define other integration operator (with the subscript "in")

$$\Pi_{(\mathrm{in})}(\tilde{u}_j(x) \to g_i(\xi)) = \frac{1}{2}\tilde{u}_i(\xi) - \int_\Gamma P^*_{ij}(\xi, x)\tilde{u}_j(x)\mathrm{d}s(x), \quad (i = 1, 2, \xi \in \Gamma). \tag{A3}$$

It is known that the operator $\Pi_{(\mathrm{in})}$ has the property

$$\Pi_{(\mathrm{in})}(b^{(k)}_j(x) \to g_i(\xi)) = \frac{1}{2}b^{(k)}_i(\xi) - \int_\Gamma P^*_{ij}(\xi, x)b^{(k)}_j(x)\mathrm{d}s(x) = 0, \quad (i = 1, 2, \xi \in \Gamma, k = 1, 2, 3) \tag{A4}$$

or

$$\frac{1}{2}b^{(k)}_i(\xi) = \int_\Gamma P^*_{ij}(\xi, x)b^{(k)}_j(x)\mathrm{d}s(x), \quad (i = 1, 2, \xi \in \Gamma, k = 1, 2, 3) \tag{A5}$$

for the following three displacement vectors:

$$\left\{\begin{array}{c} b^{(1)}_1 \\ b^{(1)}_2 \end{array}\right\} = \left\{\begin{array}{c} 1 \\ 0 \end{array}\right\}, \quad \left\{\begin{array}{c} b^{(2)}_1 \\ b^{(2)}_2 \end{array}\right\} = \left\{\begin{array}{c} 0 \\ 1 \end{array}\right\}, \quad \left\{\begin{array}{c} b^{(3)}_1 \\ b^{(3)}_2 \end{array}\right\} = \left\{\begin{array}{c} -y_t \\ x_t \end{array}\right\}, \quad (t = x_t + \mathrm{i}y_t \in \Gamma). \tag{A6}$$

The physical meaning of Eq. (A4) is as follows. In the interior boundary value problem, for the vanishing boundary tractions, the relevant displacements on the boundary are rigid translation or rotation.

By using Eqs. (A4) or (A5), we will find the following equality:

$$\Pi_{(\mathrm{ex})}\left(b^{(k)}_j(x) \to g_i(\xi)\right) = \frac{1}{2}b^{(k)}_i(\xi) + \int_\Gamma P^*_{ij}(\xi, x)b^{(k)}_j(x)\mathrm{d}s(x) = b^{(k)}_i(\xi), \quad (i = 1, 2, \xi \in \Gamma, k = 1, 2, 3). \tag{A7}$$

This ends the derivation.

References

1. Rizzo, F.J.: An integral equation approach to boundary value problems in classical elastostatics. Quart. J. Appl. Math. **25**, 83–95 (1967)
2. Cruse, T.A.: Numerical solutions in three-dimensional electrostatics. Int. J. Solids Struct. **5**, 1259–1274 (1969)
3. Brebbia, C.A., Tells, J.C.F., Wrobel, L.C.: Boundary Element Techniques—Theory and Application in Engineering. Springer, Heidelberg (1984)
4. Cheng, A.H.D., Cheng, D.S.: Heritage and early history of the boundary element method. Eng. Anal. Bound. Elem. **29**, 286–302 (2005)
5. Chen, J.T., Lin, S.R., Chen, K.H.: Degenerate Scale problem when solving Laplace's equation by BEM and its treatment. Int. J. Numer. Methods Eng. **62**, 233–261 (2005)

6. He, W.J., Ding, H.J., Hu, H.C.: Degenerate scale and boundary element analysis of two dimensional potential and elasticity problems. Comput. Struct. **60**, 155–158 (1996)
7. Vodička, R., Mantič, V.: On solvability of a boundary integral equation of the first kind for Dirichlet boundary value problems in plane elasticity. Comput. Mech. (2008, to appear). doi:10.1007//s00466-007-0202-x
8. Chen, J.T., Kuo, S.R., Lin, J.H.: Analytical study and numerical experiments for degenerate scale problems in the boundary element method of two-dimensional elasticity. Int. J. Numer. Methods Eng. **54**, 1669–1681 (2002)
9. Chen, Y.Z., Wang, Z.X., Lin, X.Y.: Eigenvalue and eigenfunction analysis arising from degenerate scale problem of BIE in plane elasticity. Eng. Anal. Bound. Elem. **31**, 994–1002 (2007)
10. Chen, Y.Z.: Analysis of L-integral and theory of the derivative stress field in plane elasticity. Int. J. Solids Struct. **40**, 3589–3602 (2003)
11. Buecker, H.F.: Field singularities and related integral representation In: Sih, G.C. (ed.) Mechanics of Fracture, vol. 1, pp. 239–314. Noordhoof, Amsterdam (1973)
12. Muskhelishvili, N.I.: Some Basic Problems of Mathematical Theory of Elasticity. Noordhoof, Amsterdam (1953)
13. Chen, Y.Z.: An accurate technique for evaluating stress at boundary points in boundary element method. Eng. Anal. Boun. Elem. **24**, 357–360 (2000)